ters Dp >3 nm (TSI 3025), radial differential mobility analyzer (RDMA) size distribution Dp 8 to 250 nm, and a laser optical particle counter (OPC-PMS LAS-X) size distribution Dp, 150 to 7000 nm. RDMA dry surface areas at about 25% RH can be multiplied by about 3 to estimate ambient surface areas at 94% RH.

17. Measurements of OH and H_2SO_4 were recorded on a selected-ion chemical-ionization mass spectrometer [F. Eisele and D. Tanner, *J. Geophys. Res.* **96**, 9295 (1991); *ibid.* **98**, 9001 (1993)]. Two sigma uncertainties on individual 1-s measurements of H_2SO_4 are ±42% (precision is 20%) but are much reduced for the 15-s averages used here [R. L. Mauldin *et al.*, *ibid.* **101**, 16713 (1998)]. SO_2 and DMS measurements were made with an isotopic-dilution gas-chromatography mass spectrometer [A. Bandy *et al.*, *ibid.* **98**, 23423 (1993)]. The photochemically related parameters CO, H_2O, NO, O_3, NMHCs, and UV irradiance were continuously recorded as were the meteorological parameters RH and *T*; for details see (J. Hoell *et al.*, *ibid.*, in press). The above species and parameters were typically measured and averaged over times ranging from 15 s to 5 min. A subset of these (for example, vertical and horizontal winds, dew point, and temperature) was high-resolution 20-Hz data.
18. The time-dependent photochemical box model for diel trends in OH is similar to that described by D. Davis *et al.* [*J. Geophys. Res.* **101**, 211 (1996)] and J. Crawford *et al.* [*ibid.* **102**, 28447 (1997)]. The chemical model assumed all calculated species to be in photochemical equilibrium and included 50 standard HOx-NOx-CH_4 reactions, 118 NMHC reactions, 15 photolytic reactions, and heterogeneous removal of soluble species. It was constrained by input values for O_3, CO, CH_4, NMHCs, NO, H_2O, temperature, pressure, and, when available, measurements of the longer lived species H_2O_2, CH_3OOH, HNO_3, and peroxyacetyl nitrate. Photolysis rates were calculated with the National Center for Atmospheric Research community radiative transfer code configured for four-stream DISORT calculations. Calculated *J* values were scaled for cloud effects based on a comparison of the observed OH with model estimated values (typically 10%).
19. G. Chen *et al*, *J. Geophys. Res*, in press.
20. D. Davis *et al.*, *ibid.*, in press.
21. The DMS flux was estimated by using a mass conservation equation with measured DMS and OH values and model-generated diel profiles for NO_3—$d[DMS]/dt$ = FDMS/EMD − (kOH[OH] + kNO_3 $[NO_3]$) [DMS]. The first term on the right-hand side is the DMS source term (sea-to-air flux), which depends on the oxidation rate of DMS and the equivalent mixing depth (EMD) (*19, 20*). The latter can be viewed as the height of an atmospheric column that contains all DMS mass (both buffer and boundary layers) but at BL concentrations. The DMS oceanic flux is balanced by a comparable loss by reaction with OH and NO_3 calculated from the 24-hour profiles for DMS, OH, and NO_3. For flight 19 the OH profile was generated independently from an O_3/HOx/NOx/CH_4 photochemical box model constrained both by the measured photochemical controlling parameters O_3, H_2O, CO, NO, NMHCs, UV, and *T* and by the limited in situ BL OH measurements (*18*). Evaluation of the EMD (1.3 km for flight 19) was based on the vertical concentration data for DMS and CH_3I (*17, 31*). Using our estimated BL height of 0.6 km, about half the DMS released had been transported into the overlying cloud layer and lower free troposphere.
22. S. Yvon *et al.*, *J. Geophys. Res.* **101**, 6899 (1996).
23. A. R. Bandy *et al.*, *Geophys. Res. Lett.* **23**, 741 (1996).
24. B. Huebert *et al.*, *J. Geophys. Res.* **98**, 16985 (1993).
25. T. Bates *et al.*, *ibid.* **92**, 2930 (1987).
26. The sulfur model used in this study is similar to that previously described (*17, 19, 31*) and is based on 14 sulfur reaction processes, five having two or more branches. Coupled sets of time-dependent continuity equations (with parameterized transport terms) are integrated to yield time-dependent concentration profiles of sulfur species. The general form of this equation is: $d[S]_{BL}/dt = Fsa/h + M/h \times ([S]_{BuL} - [S]_{BL}) + P(S) - L(S)[S]_{BL} - k(SL)[S]_{BL}$. Here $[S]_{BL}$ represents the BL concentration of a given sulfur species (DMS, SO_2, MSA, H_2SO_4), $[S]_{BuL}$ is the concentration of the sulfur species in the buffer layer, *Fsa* is the sea-to-air flux of S (DMS), *h* is the marine BL height, *M* is the mixing parameter where $M = K/z$, P(S) is the photochemical production of sulfur species S, L(S) is the photochemical loss of sulfur species S, and k(SL) is the removal of S via aerosol (dry and wet) scavenging or dry deposition. The aerosol sticking coefficient for H_2SO_4 (*20*) was derived from data collected near Christmas Island in the tropical Pacific during P3-B mission 7 of PEMT.
27. D. Davis *et al.*, *J. Geophys. Res.* **103**, 1657 (1998).
28. A. S. Wexler, F. W. Lurmann, J. H. Seinfeld, *Atmos. Environ.* **28**, 531 (1994).
29. V. Kerminen and A. Wexler, *J. Geophys. Res.* **99**, 25607 (1994).
30. L. M. Russell, S. N. Pandis, J. H. Seinfeld, *ibid.*, p. 20989.
31. D. Davis *et al.*, Fall Meeting (American Geophysical Union, San Francisco, CA, 1997).
32. W. A. Hoppel, G. M. Frick, R. E. Larson, *Geophys. Res. Lett.* **13**, 125 (1986).
33. R. J. Weber *et al.*, *Chem. Eng. Commun.* **151**, 53 (1996).
34. A. D. Clarke and J. N. Porter, *J. Geophys. Res.* **98**, 16997 (1993).
35. P. K. Quinn, T. S. Bates, J. E. Johnson, D. S. Covert, R. J. Charlson, *ibid.* **95**, 16405 (1990).
36. The growth times for new nuclei over marine regions have been shown (*37*) to be inversely proportional to H_2SO_4(g) and α. It was also shown that for a fixed H_2SO_4(g) source strength the growth rate is independent of α because H_2SO_4(g) is inversely proportional to α. Because H_2SO_4(g) and its variation at the time of nucleation is unknown we have used a range of α to provide a plausible range of growth times.
37. W. A. Hoppel, G. M. Frick, J. W. Fitzgerald, R. E. Larson, *J. Geophys. Res.* **99**, 14443 (1994).
38. Supported by NASA grants NAG-1-1764 and NAG-1-1769. This is contribution 4687 from the School of Earth Science and Technology, University of Hawaii.

9 June 1998; accepted 27 August 1998

Synchronous Climate Changes in Antarctica and the North Atlantic

E. J. Steig,*† E. J. Brook, J. W. C. White, C. M. Sucher, M. L. Bender, S. J. Lehman, D. L. Morse, E. D. Waddington, G. D. Clow

Central Greenland ice cores provide evidence of abrupt changes in climate over the past 100,000 years. Many of these changes have also been identified in sedimentary and geochemical signatures in deep-sea sediment cores from the North Atlantic, confirming the link between millennial-scale climate variability and ocean thermohaline circulation. It is shown here that two of the most prominent North Atlantic events—the rapid warming that marks the end of the last glacial period and the Bølling/Allerød–Younger Dryas oscillation—are also recorded in an ice core from Taylor Dome, in the western Ross Sea sector of Antarctica. This result contrasts with evidence from ice cores in other regions of Antarctica, which show an asynchronous response between the Northern and Southern Hemispheres.

Objective correlation of isotope paleotemperature records from polar ice cores has shown that some climate variations once thought to be synchronous in both hemispheres are in fact out of phase. For example, the Antarctic Cold Reversal (ACR), a period of cooling that appears in many Antarctic stable isotope records (*1*), has been compared with the Younger Dryas (YD), a prominent feature in Northern Hemisphere records (*2*). Time series for the cores from Vostok and Byrd Station, Antarctica, correlated to the layer-counted records in central Greenland by measurements of atmospheric trace gas concentrations in trapped air bubbles, show that the ACR occurred at least 1000 years before the YD (*3, 4*).

Geochemical climate proxies (*5, 6*) from an ice core at Taylor Dome (77°48′S, 158°43′E, 2374 m above sea level), a near coastal East Antarctic site at the western edge of the Ross Sea (Fig. 1), exhibit large fluctuations during the last glacial-interglacial transition and Holocene that are reminiscent of those in central Greenland. Published records from Taylor Dome, however, use a preliminary time scale (*6*) that precludes definitive

E. J. Steig, J. W. C. White, S. J. Lehman, Institute of Arctic and Alpine Research, University of Colorado, Boulder, CO 80309, USA. E. J. Brook, Department of Geology, Washington State University, Vancouver, WA 98686, USA. C. M. Sucher, Graduate School of Oceanography, University of Rhode Island, Narragansett, RI 02882, USA. M. L. Bender, Department of Geosciences, Princeton University, Princeton, NJ 08544, USA. D. L. Morse, Institute for Geophysics, University of Texas, Austin, TX 78759, USA. E. D. Waddington, Geophysics Program, University of Washington, Seattle, WA 98195, USA. G. D. Clow, United States Geological Survey, Denver Federal Center, Englewood, CO 80225, USA.

*To whom correspondence should be addressed. E-mail: steig@colorado.edu

†Present address: Department of Earth and Environmental Science, University of Pennsylvania, Philadelphia, PA 19104, USA.

conclusions regarding the timing of rapid climate change events. Here we present a new stable isotope (δD) record (Fig. 2) and a new chronology for the last glacial-interglacial transition in the Taylor Dome core. We use both atmospheric methane (CH_4) and the isotopic ratio of molecular oxygen ($\delta^{18}O_{atm}$) to tie Taylor Dome to the layer-counted chronology of the Greenland Ice Sheet Project 2 (GISP2) (Summit, Greenland) ice core (*7*). This approach requires calculation of the age difference (Δage) between the ice and the younger gas it encloses. For GISP2, we use the gas-age time scale and Δage values of Brook *et al.* (*8*). For Taylor Dome, we obtain a gas chronology by visually matching changes in CH_4 and $\delta^{18}O_{atm}$ concentrations with those at GISP2 (Fig. 3). The rapid increases in CH_4 before and after the YD provide precise correlation points at 14.6 and 11.6 thousand years before the present (kyr B.P.) (*9*). The precision of the correlation between 20 and 15 kyr B.P., during which both CH_4 and $\delta^{18}O_{atm}$ change relatively slowly, is between 500 and 1500 years.

We calculate Δage for Taylor Dome as a function of the effective bubble close-off depth (COD), surface temperature (T) and accumulation rate ($\dot{b}$), using the empirical Herron-Langway model to describe the firn densification process (*10*). We assume that the COD occurs at a density $\rho_{COD} = 800 \pm 10$ kg m^{-3}, as determined from nitrogen isotope ($\delta^{15}N$) measurements in firn air (*11*). Measured $\delta^{15}N$ in Taylor Dome ice samples independently constrains Δage by giving a measure of the thickness of the diffusive zone through which gravitational fractionation is manifested. Diffusive layer thicknesses calculated from measured $\delta^{15}N$ provide a minimum estimate of the COD and therefore of Δage for given T and $\dot{b}$ (*12*).

Values for T and $\dot{b}$ are taken as averages over an interval approximating the original thickness of the firn column (*13*). We assume that T is a linear function of δD, where the slope $\alpha = 4.0 \pm 1.5‰$ °C^{-1} (*14*). We calculate $\dot{b}$ from the ^{10}Be concentration (Fig. 2), where we assume that the dry deposition flux is constant and include a term for wet deposition (*15*). The ^{10}Be method is supported by several observations. First, ^{10}Be concentration and $\dot{b}$ show a strong spatial inverse correlation both locally at Taylor Dome and broadly across the Antarctic continent (*16*). Second, both empirical and theoretical considerations indicate that the dry deposition flux of ^{10}Be at polar latitudes varied little over the last glacial cycle, for averages over time intervals greater than a few decades (*17*). Third, comparison of ^{10}Be with major ion concentrations in the Taylor Dome core shows a high degree of correlation; variation in accumulation rate produces strong covariance among chemical species, including ^{10}Be and sulfate, which have very different source functions (*18*). Finally, flow model calculations, based on high-resolution radar profiles and vertical and surface velocity data, provide independent validation of ^{10}Be-based estimates of accumulation rates (*19*). For comparison, we also determine $\dot{b}$ using calculated values for T (from measured δD) by assuming that $\dot{b}$ varies as a linear function of the saturation vapor pressure of water over ice (*20*). This more commonly used approach, although probably valid for continental sites such as Vostok, is difficult to justify at Taylor Dome, where precipitation is strongly influenced by cyclonic activity (*21*); relative to the ^{10}Be method, it generally overestimates accumulation rates (and therefore underestimates Δage) during cold periods. Values of Δage calculated by the different methods vary by up to ±750 years (Fig. 3). The variance in Δage is greatest in the oldest part of the record (20 to 15 kyr B.P.) but is <300 years during the crucial YD time period and early Holocene and <600 years at 14.6 kyr B.P., at the time of the rapid deglacial warming in the Northern Hemisphere.

We obtain a time scale for Taylor Dome by adding Δage to the gas ages from correlation with GISP2, using the maximum of the estimates shown in Fig. 3. As will become apparent, this approach is the most conservative for comparing Taylor Dome with other ice core records, because it gives the oldest age for a given depth. We estimate the precision of this time scale by propagating uncertainties in ρ_{COD}, T, and $\dot{b}$ (*11, 14, 15*) and adding estimated uncertainties arising from the GISP2 age calculation and the curve-matching technique (*22*). The resulting δD time series, from 20 to 10 kyr B.P., is compared in Fig. 4 with δD at GISP2. Also shown are $\delta^{18}O$ at Byrd and δD at Vostok, both on the Sowers and Bender (*3*) time scales tied to GISP2 through $\delta^{18}O_{atm}$. For Byrd, where uncertainties in Δage are small, the time scales of both Sowers and Bender (*3*) and Blunier *et al.* (*4*) are in excellent agreement. For Vostok, uncertainties in Δage are considerably larger; ages from (*3*) are up to 1200 years greater than those from (*4*) over the interval from 20 to 10 kyr B.P.

Figure 4 illustrates three particularly important findings. First, prominent features of the GISP2 record that are absent at Byrd and Vostok appear at Taylor Dome, including

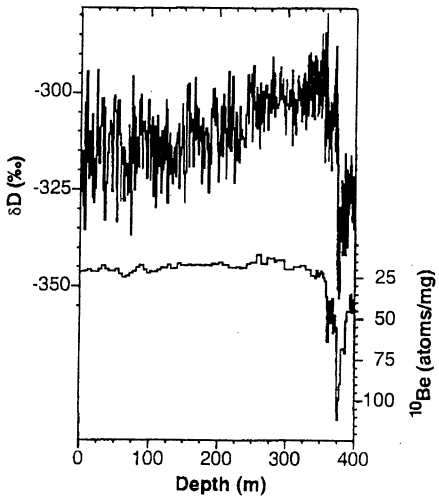

Fig. 2. δD and ^{10}Be concentrations in the Taylor Dome ice core from 0 to 400 m depth (total depth = 554 m), covering the Holocene and last glacial-interglacial transition.

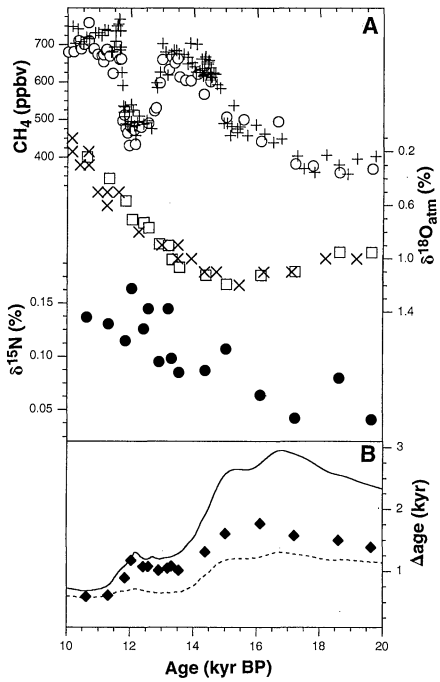

Fig. 3. (**A**) CH_4 (○), $\delta^{18}O_{atm}$ (□), and $\delta^{15}N$ (●) from trapped air bubbles in the Taylor Dome and GISP2 (+ and ×) cores. (**B**) Lines show Δage calculated using $\dot{b}$ from ^{10}Be (solid line) and δD (dashed line). Diamonds (◆) show minimum ^{10}Be Δage constrained by $\delta^{15}N$, assuming a 10-m-thick advective layer at the top of the firn column.

Fig. 1. Map of Antarctica showing locations of Antarctic ice cores.

generally declining isotope values between 20 and 15 kyr B.P. and near-Holocene isotope values during the Bølling/Allerød (B/A) warm period (14.6 to 12.9 kyr B.P.). Second, the late-glacial cold interval (low δD values) at Taylor Dome, although more subdued than at GISP2, is at least approximately contemporaneous with the Northern Hemisphere YD and definitely lags the ACR. This interval ends with a rapid warming that is synchronous with post-YD warming at GISP2 within a few hundred years. Third, the dramatic warming that marks the end of the last glacial maximum at Taylor Dome lags the onset of gradual warming at Vostok and Byrd by more than 3000 years. In the latter cores, deglacial warming begins before 18 kyr B.P. and continues uninterrupted until the ACR cooling. At GISP2 there is evidence for an initiation of warming as early as 24 kyr B.P., but isotope values generally indicate cold conditions until nearly 14.6 kyr B.P., when rapid deglacial warming occurred. At Taylor Dome, the magnitude of the δD increase during deglacial warming is as large as at GISP2. Uncertainties in both time scales over this interval are considerably larger than for the B/A and YD, but the precision is sufficient to conclude that deglacial warming was synchronous in both cores within 1000 years.

Evidently, climate changes at Taylor Dome during the last glacial-interglacial transition were synchronous or near synchronous with changes in the North Atlantic region. This result has important implications for our understanding of the mechanisms linking climate between the hemispheres. It is generally accepted that abrupt deglacial warming in the Northern Hemisphere was accompanied by the onset of North Atlantic deep water (NADW) formation, promoting northward flow of warm surface waters from the tropics, whereas a circulation pattern marked by reduced NADW formation accounts for cold conditions during the YD interval (*23*). The Byrd and Vostok records, showing an antiphase relationship between Antarctica and Greenland, have drawn attention to numerical model results in which changes in NADW promote opposing temperature responses in the high latitudes of the Northern and Southern Hemispheres, a consequence of an alternation in the amount of convection or ocean heat convergence (or both) in the two areas (*24*). The Taylor Dome results, on the other hand, are consistent with earlier arguments that the flow of relatively warm NADW into the Southern Ocean warms circumpolar deep water (CPDW), thereby promoting sea ice melting and atmospheric warming as CPDW upwells along the Antarctic coastal margin (*25*).

Differences between the isotope-temperature history from Taylor Dome and those from other Antarctic sites are too large to be attributed to dating errors. Rather, the results indicate that the circum-Antarctic climate response to changes in NADW formation and export may not be uniform. We propose that the North Atlantic character of the isotopic record at Taylor Dome, in particular, reflects the relative proximity of this site to the western Ross Sea, an area of active wind-driven convection and ocean-atmosphere heat exchange in today's climate (*26*). We note that a similarly heterogeneous response to transient reduction of NADW formation and export has been observed in some numerical models (*27*). For example, in the coupled atmosphere-ocean general circulation model simulations of Schiller *et al.* (*28*), near-Antarctic waters of the Southern Ocean (areas of vigorous oceanic convection in control simulations) cool in response to reduced formation and export of NADW, whereas other areas of the Southern Ocean warm as a result of changing patterns of atmospheric circulation and increased ocean heat convergence. Taylor Dome may thus record the direct but localized influence of NADW-borne heat on Antarctic climate (*29*). Given the substantial difficulty of realistically simulating ocean-atmosphere interactions in general, and the dynamics of the Southern Ocean in particular, it may be some time before the role of NADW in shaping Antarctic climate can be rigorously evaluated. In the meantime, our observations can and should be tested by collection and analysis of additional Antarctic ice cores, especially from near-coastal sites.

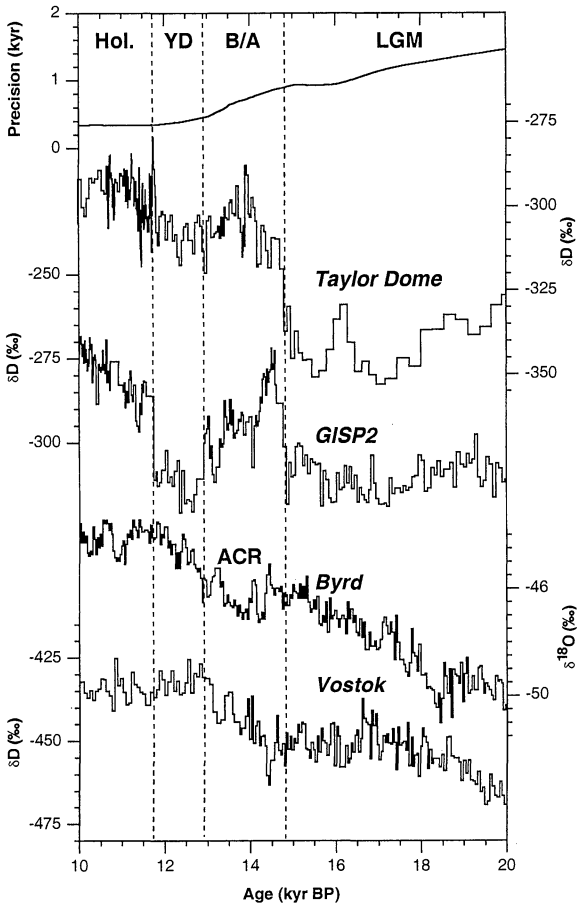

Fig. 4. Stable isotope profiles from Taylor Dome, GISP2, Byrd, and Vostok. At the top, the estimated precision in the Taylor Dome age scale is shown [alternative calculations of Δage (Fig. 3) produce younger ages, increasing the contrast with other Antarctic cores]. Boundaries of climate intervals, as defined in the GISP2 record, are shown by dashed vertical lines Hol, Holocene; YD, Younger Dryas; B/A, Bølling/Allerød; LGM, last glacial maximum. ACR is the Antarctic Cold Reversal as defined at Byrd (*4*).

References and Notes

1. J. Jouzel *et al.*, *NATO ASI Series* **I2**, 229 (1992); *Clim. Dyn.* **11**, 151 (1995).
2. S. J. Johnsen *et al.*, *Nature* **359**, 311 (1992); P. M. Grootes *et al.*, *ibid.* **366**, 552 (1993).
3. M. Bender *et al.*, *ibid.* **372**, 663 (1994); T. Sowers and M. Bender, *Science* **269**, 210 (1995).
4. T. Blunier *et al.*, *Geophys. Res. Lett.* **24**, 2683 (1997); *Nature* **394**, 739 (1998).
5. P. A. Mayewski *et al.*, *Science* **272**, 1636 (1996); J. C. Stager and P. A. Mayewski, *ibid.* **276**, 1834 (1997); E. J. Steig *et al.*, *Ann. Glaciol.*, in press. The original time scale used in these papers, *st9507* (*6*), is based on preliminary flow model calculations and a visual match between Taylor Dome $\delta^{18}O$ [P. M. Grootes, E. J. Steig, M. Stuiver, E. D. Waddington, D. L. Morse, *Eos* **75**, 225 (1994)] and Vostok δD [J. Jouzel *et al.*, *Nature* **364**, 407 (1993)].
6. E. J. Steig, thesis, University of Washington, Seattle (1996).
7. R. B. Alley *et al.*, *Nature* **362**, 527 (1993). The $\delta^{18}O_{atm}$ values were corrected for gravitational fractionation using $\delta^{15}N$, as described [T. Sowers, M. Bender, D. Raynaud, *J. Geophys. Res.* **94**, 5137 (1989)].
8. E. J. Brook, T. Sowers, J. Orchado, *Science* **273**, 1087 (1996).
9. J. P. Severinghaus *et al.*, *Nature* **391**, 141 (1998).
10. M. M. Herron and C. C. Langway, *J. Glaciol.* **25**, 373 (1980).
11. $\delta^{15}N$ rises through most of the firn column as a result of gravitational fractionation [H. Craig, Y. Horibe, T.

Sowers, *Science* **242**, 1675 (1988)]. It ceases to rise near the base of the firn when dense layers begin to close off, preventing further diffusion. At Taylor Dome, $\delta^{15}N$ values typical of Holocene ice [~0.25 per mil (‰)] are reached at a firn density of 800 kg m^{-3} [C. M. Sucher, thesis, University of Rhode Island, Narragansett (1997)]. This value is about 2% lower than that obtained at GISP2 or the South Pole [M. Battle *et al.*, *Nature* **383**, 231 (1996)].

12. T. Sowers, M. Bender, D. Raynaud, Y. S. Korotkevich, *J. Geophys. Res.* **97**, 15683 (1992).
13. The original firn thickness is assumed to be 50 m (ice equivalent depth). Thinning due to glacier flow was calculated as described [E. D. Waddington, D. L. Morse, P. M. Grootes, E. J. Steig, *NATO ASI Ser.* **I12**, 499 (1993); D. L. Morse, thesis, University of Washington, Seattle (1997)].
14. The equation $\alpha = 4‰°C^{-1}$ (equivalent to $0.5‰°C^{-1}$ for $\delta^{18}O$) agrees with borehole temperature analyses at Taylor Dome showing a ~1.5° cooling at Taylor Dome since about 4 kyr B.P., during which δD dropped by ~6‰ [E. D. Waddington and G. D. Clow, *Eos Trans.* **78**, F41 (1997)]. Varying α by $\pm 1.5‰°C^{-1}$ simulates possible temporal changes [K. M. Cuffey *et al.*, *Science* **270**, 455 (1995)].
15. $\dot{b}$ at depth z is given by $F_{dry}/([^{10}Be](z) - [^{10}Be]_{wet})$, where $[^{10}Be]_{wet} = 5 \pm 5$ atoms mg^{-1} (*6*) is the concentration of ^{10}Be in wet precipitation, and $F_{dry} = \dot{b}(0)([^{10}Be](0) - [^{10}Be]_{wet})$ is the dry-deposition flux.
16. E. J. Steig, P. J. Polissar, M. Stuiver, *Antarct. J. U. S.* **30**, 95 (1995); G. M. Raisbeck and F. Yiou, *Ann. Glaciol.* **7**, 138 (1985).
17. E. J. Steig, P. J. Polissar, M. Stuiver, R. C. Finkel, P. M. Grootes. *Geophys. Res. Lett.* **23**, 523 (1996); E. Bard, G. M. Raisbeck, F. Yiou, J. Jouzel, *Earth Planet. Sci. Lett.* **150**, 453 (1997); R. C. Finkel and K. Nishiizumi, *J. Geophys. Res.* **102**, 26699 (1997).
18. R. B. Alley *et al.*, *J. Glaciol.* **41**, 503 (1995). In the Taylor Dome core, the correlation coefficient between ^{10}Be and SO_4 is >0.75.
19. E. J. Steig, D. L. Morse, E. D. Waddington, P. J. Polissar. *Geophys. Res. Lett.* **25**, 163 (1998).
20. G. de Q. Robin, *Philos. Trans. R. Soc. London Ser. A* **280**, 143 (1977); J. Jouzel *et al.*, *Quat. Res.* **31**, 135 (1989).
21. E. D. Waddington and D. L. Morse, *Ann. Glaciol.* **20**, 219 (1994); E. J. Steig, *ibid.* **25**, 418 (1997).
22. The uncertainty in GISP2 Δage is taken from comparison of results from two independent calculations, which are in agreement within ±100 years [(*8*) and J. Schwander *et al.*, *J. Geophys. Res.* **102**, 19483 (1997)]. Uncertainty in the curve match is taken as one-half the sampling interval, generally 1000 years for the period from 20 to 15 kyr B.P. and 150 years for the period from 15 to 10 kyr B.P.
23. S. J. Lehman and L. D. Keigwin, *Nature* **356**, 757 (1992); *ibid.* **358**, 197 (1992).
24. T. J. Crowley, *Paleoceanography* **7**, 489 (1992); T. Stocker, *ibid.* p. 529; W. S. Broecker, *Science* **278**, 1582 (1997).
25. T. J. Crowley and C. L. Parkinson, *Clim. Dyn.* **3** (1988); W. S. Broecker and G. H. Denton, *Geochim. Cosmochim. Acta* **53**, 2465 (1989); J. Imbrie *et al.*, *Paleoceanography* **7**, 701 (1993). Compatible with this explanation, $\delta^{13}C$ ratios in benthic foraminifera from deep-sea sediment cores indicate that the flux of NADW to the Southern Ocean increased abruptly at 14 to 15 kyr B.P. Moreover, the subdued nature of the B/A-YD oscillation at Taylor Dome, relative to that in the central Greenland records, parallels the relatively small benthic $\delta^{13}C$ response during this period [C. D. Charles and R. G. Fairbanks, *Nature* **355**, 416 (1992); C. D. Charles, J. Lynch-Stieglitz, U. S. Ninnemann, R. G. Fairbanks, *Earth Planet. Sci. Lett.* **142**, 19 (1996)].
26. S. S. Jacobs, R. G. Fairbanks, and Y. Horibe [*Antarct. Res. Ser.* **43**, 203 (1985)] estimate that southward oceanic heat transport provides a net flux of heat to the atmosphere of ~3 W/m^2 along the Antarctic coastal margin. Local heat fluxes from leads and polynyas in the western Ross Sea, kept open by the strong westerly katabatic wind flow [D. D. Kurtz and D. Bromwich, *ibid.*, p. 177; H. J. Zwally and J. C. Comiso, *ibid.*, p. 203], may be two orders of magnitude higher [D. J. Cavalieri and S. Martin, *ibid.*, p. 227].
27. U. Mikolajewicz *et al.*, *Nature* **387**, 384 (1997); S. Manabe and R. J. Stouffer, *Paleoceanography* **12**, 321 (1997).
28. A. Schiller, U. Mikolajewicz, R. Voss, *Max-Plank-Inst. Meteorol. Rep. 188* (1996); *Clim. Dyn.* **13**, 325 (1997).
29. The sensitivity of Taylor Dome to local oceanographic conditions may depend on ice sheet configuration, especially the position of the Ross Ice Sheet/Ice Shelf margin. Although the Ross Ice Sheet may not have reached all the way to the continental shelf break during the last glacial maximum [K. J. Licht, A. E. Jennings, J. T. Andrews, K. M. Williams, *Geology* **24**, 223 (1996)], the distance between Taylor Dome and seasonally open water would have been greater, and local atmospheric circulation patterns may have been altered [D. L. Morse, E. D. Waddington, E. J. Steig, *Geophys. Res. Lett.* **25**, 3383 (1998)]. We do not therefore expect a simple linear relation between proxies of ocean circulation and Taylor Dome δD even if, as we suggest, changes in ocean circulation are the primary forcing mechanism.
30. We thank G. Denton and M. Stuiver for suggesting an ice core at Taylor Dome, P. Grootes for directing the field program, the Polar Ice Coring Office and Antarctic Program of NSF for logistical and financial support, and R. Alley and M. Kaplan for helpful comments on the manuscript.

15 July 1998; accepted 28 August 1998

Solution Properties of Single-Walled Carbon Nanotubes

Jian Chen, Mark A. Hamon, Hui Hu, Yongsheng Chen, Apparao M. Rao, Peter C. Eklund, Robert C. Haddon*

Naked metallic and semiconducting single-walled carbon nanotubes (SWNTs) were dissolved in organic solutions by derivatization with thionychloride and octadecylamine. Both ionic (charge transfer) and covalent solution-phase chemistry with concomitant modulation of the SWNT band structure were demonstrated. Solution-phase near-infrared spectroscopy was used to study the effects of chemical modifications on the band gaps of the SWNTs. Reaction of soluble SWNTs with dichlorocarbene led to functionalization of the nanotube walls.

With novel structural, electronic, and mechanical properties, SWNTs constitute an important new form of carbon that may find applications in many fields (*1*). The functionalization chemistry of the open ends, the exterior walls (convex face), and the interior cavity (concave face) of the SWNTs is expected to play a vital role in tailoring the properties of these materials and the engineering of nanotube devices. However, all of the currently known forms of SWNT material are insoluble in organic solvents (*2, 3*), making it difficult to explore and understand the chemistry of SWNTs (*4*) at the molecular level. We report here an approach to the dissolution of shortened SWNTs (*5*) in common organic solvents. Various solution spectroscopies were applied to characterize the dissolved SWNTs. We found that the band gaps of some types of SWNTs can be measured directly by solution-phase near-infrared (IR) spectroscopy, which allows the study of the effects of chemical modifications on the band gaps of SWNTs, the key to the molecular design of new SWNT-based materials. Solution-phase wall chemistry was demonstrated by reaction of the soluble SWNTs (s-SWNTs) with dichlorocarbene. The s-SWNTs will have a rich solution chemistry, perhaps rivaling that of the fullerenes. They are versatile precursors to nanotube-based copolymers, composites, and metal ligands.

The SWNT-containing raw soot (40 to 60% purity, obtained from CarboLex Inc.) was prepared by the modified electric-arc technique (*3*). Purified SWNTs (>90%) and shortened SWNTs (100 to 300 nm in length) were obtained by the method of Smalley and co-workers (*5*). In the final step of purification, we added HCl to the aqueous suspension of SWNTs before collecting the sample, so that the opened ends of the purified SWNTs were terminated with carboxylic acid groups (–COOH, IR frequency $\nu_{C=O} = 1719$ cm^{-1}) rather than carboxylate groups ($–COO^-$, $\nu_{C=O} = 1620$ cm^{-1}) (Fig. 1). The shortened SWNTs have similar IR features. The Raman spectrum of the shortened SWNTs collected with 1064-nm excitation ($\omega_r = 161$ cm^{-1}, $\omega_t = 1595$ cm^{-1}, where ω_r and ω_t are the Raman-active radial mode and tangential mode frequencies of SWNTs, respectively) is close to that of raw soot ($\omega_r = 162$ cm^{-1}, $\omega_t = 1592$ cm^{-1}). The Raman radial mode of the SWNTs is sensitive to the diameter *d* but not to the symmetry of the nanotube (*6, 7*); hence, if ω_r (cm^{-1}) = 223.75

Departments of Chemistry and Physics, Center for Applied Energy Research and Advanced Carbon Materials Center, University of Kentucky, Lexington, KY 40506, USA.

*To whom correspondence should be addressed. E-mail: haddon@pop.uky.edu